High Energy Density Physics 20 (2016) 1–8

Contents lists available at ScienceDirect

High Energy Density Physics

journal homepage: www.elsevier.com/locate/hedp

On the Optimized Atomic Exchange Potential method and the CASSANDRA opacity code

M. Jeffery *, J.W.O. Harris, D.J. Hoarty

AWE, Aldermaston, Berkshire, United Kingdom

ARTICLE INFO

Article history:
Received 19 January 2016
Received in revised form 27 April 2016
Accepted 29 April 2016
Available online 4 May 2016

Keywords:
CASSANDRA
Exchange potential
Optimized Atomic Central Potential Method
Plasma opacity
Atomic spectra
Janak's Theorem

ABSTRACT

The CASSANDRA, average atom, opacity code uses the local density approximation (LDA) to calculate electron exchange interactions and this introduces inaccuracies due to the inconsistent treatment of the Coulomb and exchange energy terms of the average total energy equation. To correct this inconsistency, the Optimized Atomic Central Potential Method (OPM) of calculating exchange interactions has been incorporated into CASSANDRA. The LDA and OPM formalisms are discussed and the reason for the discrepancy when using the LDA is highlighted. CASSANDRA uses a Taylor series expansion about an average atom when computing transition energies and uses Janak's Theorem to determine the Taylor series coefficients. Janak's Theorem does not apply to the OPM; however, a corollary to Janak's Theorem has been employed in the OPM implementation. A derivation of this corollary is provided. Results of simulations from CASSANDRA using the OPM are shown and compared against CASSANDRA LDA, DAVROS (a detailed term accounting opacity code), the GRASP2K atomic physics code and experimental data.

1. Introduction

There exists a long standing problem with opacity codes, such as CASSANDRA [1,2], that use the local density approximation (LDA) [3] whereby orbital transition energies, most notably those involving s-state orbitals, are incorrectly calculated. The underlying issue, identified by Wilson et al. [4], is the spurious self interaction energy inherent in both the Coulomb and exchange terms of the total energy equation. The self interaction of these two terms might be expected to cancel exactly, but this is not the case because the Coulomb potential and exchange potential are not calculated in a consistent manner; the Coulomb potential is an exact calculation whilst the exchange potential is an approximation, so the two are quantitatively different. This is outlined in Section 2.

There are many methods of self interaction correction, primarily based on an original idea by Perdew and Zunger [5]. These methods apply a correction scheme, with varying levels of success, rather than solving the root cause of the problem. Other methods exist for dealing with the exchange potential, notably that of Krieger, Li and Iafrate [6] and Becke and Johnson [7]. Both use an approximation to the Optimized Atomic Central Potential Method (OPM) of Talman and Shadwick [8–10] and are remarkably accurate, but not exact. The reason for the various approaches is the computational expense of obtaining an exact exchange potential. However, given the advances in computational efficiency to date, it is now a practical option to address the root cause rather than using a correction or an approximate method.

To obtain accurate atomic energies the exchange potential must be calculated in a manner consistent with the Coulomb potential. Prompted by Wilson et al. [4], the Optimized Atomic Central Potential Method of Talman and Shadwick has been incorporated into CASSANDRA to compute the exchange term of the configuration average total energy equation in a manner that is consistent with the Coulomb term whilst retaining the ability to calculate energy differentials from a semi-analytical form. As a result of this work CASSANDRA now provides a consistent treatment of self interaction in the Coulomb and exchange calculations and produces transition energies that compare favourably with experimental data and other opacity code simulations. In Section 5, results from CASSANDRA LDA and CASSANDRA OPM simulations are compared with experiments originating from the HELEN laser [11] and with simulations from DAVROS [12], a detailed term accounting opacity code independently developed at AWE. Calculations of transition energies are also compared with GRASP2K [13], a Multi-Configuration Dirac–Hartree–Fock atomic structure package, known for its accuracy in determining line positions and regularly used as a point of reference, for example [4,12].

* Corresponding author. AWE, Aldermaston, Berkshire, United Kingdom.
E-mail address: michael.jeffery@awe.co.uk (M. Jeffery).

http://dx.doi.org/10.1016/j.hedp.2016.04.002
1574-1818/

To reduce the number of Self-Consistent Field (SCF) calculations and thus the computational time required to determine orbital transition energies, CASSANDRA uses a Taylor series expansion about an average atom [14], for which the coefficients are determined according to Janak's Theorem [15]. Use of the LDA formalism ensures that Janak's Theorem is satisfied. The OPM does not obey Janak's Theorem so, for CASSANDRA to make use of the OPM, a corollary must be derived. This is discussed in detail in Sections 3 and 4.

2. The LDA exchange and discrepancies in self interaction energy

Discrepancies with the LDA have been the subject of prior work and the reader is referred to Wilson et al. [4] for a more comprehensive discussion. This section provides an outline of the issues involved.

Using the LDA formalism of CASSANDRA, the configuration average total energy is a summation of the kinetic and potential energy of the orbitals:

$$E_{Ave} = E_K - E_N + \frac{1}{2}\int\int dr dr' \frac{\rho(r)\rho(r')}{|r'-r|} + \int dr \rho(r)\varepsilon_{xc}[\rho(r)] \tag{1}$$

where ρ denotes the bound electron charge density:

$$\rho(r) = \sum_i n_i |\Psi_i(r)|^2 \tag{2}$$

E_K and E_N are the kinetic and nuclear potential energy respectively. The third term is the Coulomb energy and the fourth denotes the exchange energy, with ε_{xc} representing the exchange and correlation energy density, the form of which is unknown, but is assumed to be a function of the bound electron charge density. The subscript i refers to the orbital number, with n_i being the occupancy of the orbital and $\Psi_i(r)$ being the orbital wave function. The r and r′ are position operators of two bound electrons.

The issue with this formulation is the failure of both the Coulomb interaction and the exchange interaction to vanish for a one electron ion, which is entirely due to the spurious self interaction inherent in the third and fourth terms of Eq. (1), the physical interpretation of which is that the electron is interacting with itself, which is clearly incorrect.

Given that both terms contain a self interaction component, it might be expected that the self interaction would naturally cancel because they are functions of the same charge density. However, the exchange potential and the Coulomb potential are not calculated in the same manner, that is, one is an exact calculation based on the wave functions and the other is an approximation founded on the electron density and so the cancellation is not exact. As a consequence, the total average energy, E_{ave}, is not completely free of self interaction and this results in discrepancies in calculated transition energies. As self interaction is a function of the orbital energy, the discrepancy is larger for transitions originating from inner s-state orbitals with the discrepancy reducing for p-states and ensuing outer orbitals.

To overcome this problem of inconsistently calculated exchange and Coulomb potentials, while maintaining the ability to use the Taylor series approach to determine transition energies, the OPM form of atomic exchange has been incorporated into CASSANDRA.

3. The importance of Janak's Theorem

To accurately model monochromatic opacities, it is necessary to account for all probable configurations of bound electrons. To do this exactly requires that a Self-Consistent Field calculation be performed for each configuration, which, due to the computational time required, particularly with increasing atomic number, is somewhat impractical. An alternative approach is to use a Taylor series expansion to calculate the total energy of the ion for distinct occupation numbers, based on the energy of some reference configuration.

$$E(n) = E(n^*) + \sum_i a_i(n_i - n_i^*) + \frac{1}{2}\sum_{ij}(n_i - n_i^*)b_{ij}(n_j - n_j^*) \tag{3}$$

where

n_i and n_j are the occupancy of the indexed orbitals i and j;
$E(n)$ is the total energy of the ion with n bound electrons;
$E(n^*)$ is the total energy of the average atom reference configuration with n^* bound electrons;
a_i is the first derivative of the total energy with respect to the occupation number, n;
b_{ij} is the second derivative of the total energy with respect to the occupation number, n:

$$a_i = \frac{\partial E}{\partial n_i} \quad \text{and} \quad b_{ij} = \frac{\partial^2 E}{\partial n_i \partial n_j} \tag{4}$$

For CASSANDRA using the LDA, the atomic model satisfies Janak's Theorem and so the derivatives of Eq. (4) become:

$$a_i = \frac{\partial E}{\partial n_i} = \varepsilon_i \quad \text{and therefore} \quad b_{ij} = \frac{\partial \varepsilon_i}{\partial n_j},$$

where ε_i are the energy eigenvalues.

As a consequence of using an atomic model that satisfies Janak's Theorem, the Taylor series coefficients may be efficiently obtained from $N+1$ SCF calculations, where N is the number of orbitals in the problem. Conversely, calculating a_i and b_{ij} independently would require N^2 SCF calculations. The importance of Janak's Theorem in facilitating a method of rapid calculation of configuration energies is clear. If the OPM formalism is to be used with CASSANDRA, then, given that it does not satisfy Janak's Theorem, it must satisfy a corollary of Janak's Theorem.

4. A Janak type approach for the OPM

Following similar arguments to those in Janak's original paper, an alternative to Janak's Theorem can be determined for the OPM. For further insight the reader is encouraged to read Refs. 8–10,15. For the OPM, the average total energy for an isolated ion is defined as

$$E_{ave} = \sum_i n_i \left(E_i^K + E_i^N + \frac{1}{2}\int dr |\Psi_i|^2 V_{Dir} \right) - \frac{1}{2}\sum_i \int dr \Psi_i h a_i(r) \tag{5}$$

where V_{Dir} is the direct, two particle Coulomb potential. The last term is the OPM exchange energy with $ha_i(r)$ representing the orbital exchange potential; this is more clearly defined in Eqs. (13) and (14).

To construct the energy differential it is convenient to deal with the first two terms – the kinetic and nuclear potential energy terms – and then address the last two terms – the Coulomb and exchange energy terms separately. The energy derivative with respect to occupation number, n_i, of the kinetic and nuclear potential energy is trivial and can simply be noted as the sum of the kinetic and nuclear potential energy of the orbital in question:

$$\frac{\partial\left(\left[\sum_i n_i\left(E_i^K + E_i^N\right)\right]\right)}{\partial n_i} = E_i^K + E_i^N \tag{6}$$

The third term of Eq. (5), that involving V_{Dir}, is the direct two-particle Coulomb component and is complicated by the fact V_{Dir} is proportional to the occupation numbers such that:

$$V_{Dir} = 2\sum_j n_j \left(\frac{1}{r}\int_0^r dr' |\Psi_j|^2 + \int_r^\infty dr' \frac{1}{r'} |\Psi_j|^2 \right) \tag{7}$$

Therefore the direct two-particle Coulomb energy becomes:

$$E^{Dir} = \frac{1}{2}\sum_i n_i \int dr |\Psi_i|^2 \left[2\sum_j n_j \left(\frac{1}{r}\int_0^r dr' |\Psi_j|^2 + \int_r^\infty dr' \frac{1}{r'} |\Psi_j|^2 \right) \right] \tag{8}$$

For convenience, let the integral terms in the inner bracket be $f_j(r)$. Then Eq. (8) can be written as

$$E^{Dir} = \sum_i n_i \sum_j n_j \int dr |\Psi_i|^2 f_j(r) \tag{9}$$

The differential with respect to the occupation number, n_i, thus becomes:

$$\frac{\partial E^{Dir}}{\partial n_i} = 2n_i \int dr |\Psi_i|^2 f_i(r) + \sum_{j\neq i} n_j \int dr \left[|\Psi_i|^2 f_j(r) + |\Psi_j|^2 f_i(r) \right] \tag{10}$$

which, having recombined the n terms, becomes:

$$\frac{\partial E^{Dir}}{\partial n_i} = \sum_j n_j \int dr \left[|\Psi_i|^2 f_j(r) + |\Psi_j|^2 f_i(r) \right] \tag{11}$$

And given the normalization condition such that $\int |\Psi_i|^2 f_j(r) = \int |\Psi_j|^2 f_i(r)$, then this is simply the direct two-particle Coulomb energy of Eq. (5). Therefore the derivative of E_{Dir} with respect to n_i is

$$\frac{\partial E^{Dir}}{\partial n_i} = \int dr |\Psi_i|^2 V_{Dir} \tag{12}$$

Turning to the last term of Eq. (5), the exchange energy term. The exchange energy component is complicated by the fact that $ha_i(r)$ is proportional to the occupation numbers, n_i, such that:

$$E_{exc} = \frac{1}{2}\sum_i \int dr \Psi_i h a_i(r) \tag{13}$$

$$\begin{aligned} &= \frac{1}{2}\sum_i \int dr \Psi_i 2 \sum_{j\neq i} \sum_L \frac{1}{2} n_i n_j \begin{pmatrix} l_i & l_j & L \\ 0 & 0 & 0 \end{pmatrix}^2 f_{ij}(r) \Psi_j \\ &+ \frac{1}{2}\sum_i \int dr \Psi_i 2 \sum_{j=i, L=0} n_j f_{ij}(r) \Psi_j \\ &+ \frac{1}{2}\sum_i \int dr \Psi_i 2 \sum_{j=i, L\neq 0} \frac{1}{2} n_i (n_j - 1) g_{ij}(r) \Psi_j \end{aligned} \tag{14}$$

where

$$f_{ij} = \frac{1}{r^{L+1}}\int_0^r dr' \frac{r'^{L+1}}{r'} |\Psi_i \Psi_j| + \frac{r^{L+1}}{r}\int_r^\infty dr' \frac{1}{r'^{L+1}} |\Psi_i \Psi_j| \tag{15}$$

And for L.S coupling,

$$g_{ij} = \frac{2(2l_i+1)}{2(2l_i+1)-1} \begin{pmatrix} l_i & l_j & L \\ 0 & 0 & 0 \end{pmatrix} f_{ij} \tag{16}$$

$\begin{pmatrix} l_i & l_j & L \\ 0 & 0 & 0 \end{pmatrix}$ is the 3-j symbol. l_i, l_j represent the angular momentum of orbitals i and j,

$L = |l_i - l_j|, |l_i - l_j| + 2, |l_i - l_j| + 4 \ldots l_i + l_j$; see p. 164 of Ref. 16 for details.

Equation (14) has 3 component parts, each of which is calculated or omitted depending on the values of i, j and L. The first term is used when $j \neq i$ irrespective of the value of L; the second when $j = i$ and $L = 0$ and the third when $j = i$ and $L \neq 0$. A point to note at this juncture is that these equations may be further simplified, but are presented here in the form in which they are used in the original OPM code [9]. This should provide some clarity if comparisons are to be made between this implementation and the original OPM code.

From Eq. (14), the energy differential with respect to occupation number is

$$\begin{aligned} \frac{\partial E_{Exc}}{\partial n_i} &= \frac{1}{2}\sum_{j\neq i} 2n_j \int dr \sum_L \Psi_i \begin{pmatrix} l_i & l_j & L \\ 0 & 0 & 0 \end{pmatrix}^2 f_{ij}(r) \Psi_j \\ &+ \frac{1}{2}\sum_{j=i, L=0} 2 \int dr \Psi_i f_{ij}(r) \Psi_j \\ &+ \frac{1}{2}\sum_{j=i, L\neq 0} \int dr \Psi_i (2n_j - 1) g_{ij}(r) \Psi_j \end{aligned} \tag{17}$$

Combining Eqs. (6), (12) and (17) provides an equation for the differential of the total average energy (5) with respect to occupation number:

$$\begin{aligned} \frac{\partial E_{ave}}{\partial n_i} &= E_i^K + E_i^N + \int dr |\Psi_i|^2 V_{Dir} \\ &- \frac{1}{2}\sum_{j\neq i} 2n_j \int dr \sum_L \Psi_i \begin{pmatrix} l_i & l_j & L \\ 0 & 0 & 0 \end{pmatrix}^2 f_{ij}(r) \Psi_j \\ &- \frac{1}{2}\sum_{j=i, L=0} 2 \int dr \Psi_i f_{ij}(r) \Psi_j \\ &- \frac{1}{2}\sum_{j=i, L\neq 0} \int dr \Psi_i (2n_j - 1) g_{ij}(r) \Psi_j \end{aligned} \tag{18}$$

It is tempting at this point to attempt to reduce Eq. (18) to a simple one involving the orbital eigenvalue within which the complexities of the exchange energy derivative would be subsumed. However, this would require that the E_{Exc} term of Eq. (13) be valid as the exchange energy of the Schrödinger equation for each orbital and this is not the case. An equation involving the eigenvalue can be derived, but the complexities of the exchange energy component remain. For simplicity, the non-relativistic Schrödinger equation is used here, but extension to the relativistic Dirac equations is a straightforward exercise.

The Schrödinger equation for the OPM model is

$$\left[-\nabla^2 - \frac{2Z}{r} + V_{Dir}(r) + QA(r) \right] \Psi_i = \varepsilon_i \Psi_i \tag{19}$$

where

$QA(r)$ is the effective exchange potential, simply defined in Refs. 8,9 as the total potential minus the Hartree potential, $V(r)$–$V_H(r)$.

Operating on both sides of Eq. (19) with Ψ_i^*, integrating over the radial vector for the energy calculation and with reference to Eq. (18), it can be seen that the energy derivative can also be expressed as

$$\begin{aligned} \frac{\partial E_{ave}}{\partial n_i} &= \varepsilon_i - E_i^{QA} \\ &- \frac{1}{2}\sum_{j\neq i} 2 \int dr \Psi_i \sum_L n_j \begin{pmatrix} l_i & l_j & L \\ 0 & 0 & 0 \end{pmatrix}^2 f_{ij}(r) \Psi_j \\ &- \frac{1}{2}\sum_{j=i, L=0} 2 \int dr \Psi_i f_{ij}(r) \Psi_j \\ &- \frac{1}{2}\sum_{j=i, L\neq 0} \int dr \Psi_i (2n_j - 1) g_{ij}(r) \Psi_j \end{aligned} \tag{20}$$

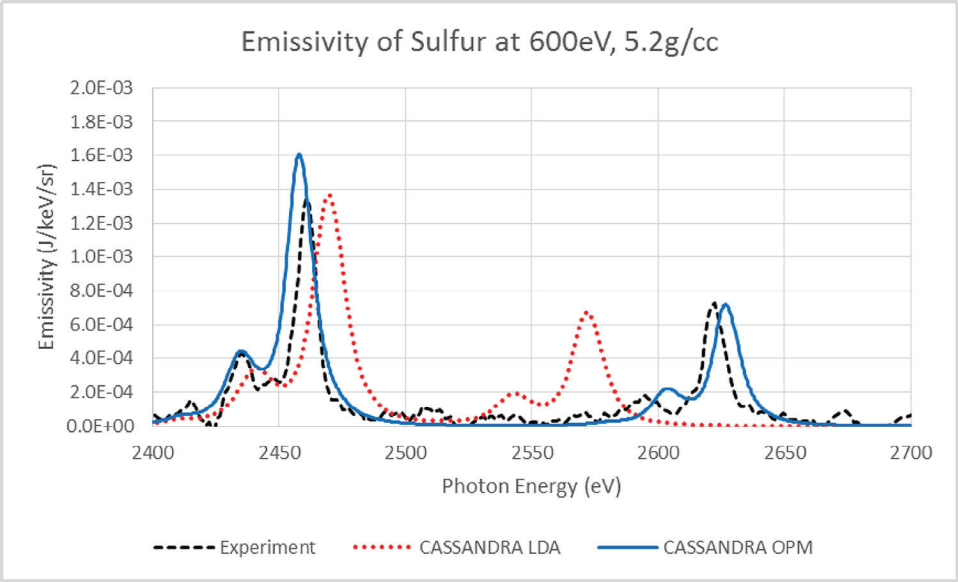

Fig. 1. Emissivity of sulfur. Comparison between experiment and CASSANDRA with the LDA and OPM exchange. The position of the experimental Ly$_\alpha$ line at 2625 eV is fairly well matched by the OPM at 2627 eV, but this feature is located at 2573 eV using the LDA exchange. The position of the experimental He$_\alpha$ line is at 2461 eV and the OPM and LDA are 2 eV lower and 9 eV higher in energy respectively.

where

$E_i^{QA} = \int dr\, \psi^* QA(r) \psi$ is the effective exchange energy of orbital i.

So, for the first derivative or the a_i coefficient of the Taylor series expansion (3), we have

$$a_i = \frac{\partial E_{ave}}{\partial n_i} = \varepsilon_i - E_i^{QA} - \frac{\partial E_{Exc}}{\partial n_i} \tag{21}$$

And for the second derivative or b_{ij} coefficient:

$$b_{ij} = \frac{\partial^2 E_{ave}}{\partial n_i \partial n_j} = \frac{\partial \varepsilon_i}{dn_j} - \frac{\partial E_i^{QA}}{dn_j} - \frac{\partial^2 E_{Exc}}{\partial n_i \partial n_j} \tag{22}$$

This confirms that the OPM does not conform to Janak's Theorem. However, the set of Eqs. (20)–(22) are a corollary of Janak's Theorem and Eqs. (21) and (22) must be used in place of the equations for a_i and b_{ij} given in Eq. (4). This ensures that the Taylor series coefficients can still be obtained from $N+1$ SCF calculations when using the OPM exchange method.

5. Results and discussion

The main test for the OPM implementation is whether the accuracy of transition energies is improved compared to the LDA formalism. To this end, comparisons with experimental data and other opacity code simulations are described. Firstly, K-shell lines for H and He like sulfur are compared to experiment, an example of niobium is compared against the DAVROS opacity code and GRASP2K line positions and finally simulations of a germanium experiment are reviewed.

5.1. Sulfur, Lyman-Alpha and He-Alpha lines: $T \approx 600$ eV, $\rho \approx 5.2$ g/cc

Fig. 1 shows a comparison between experiment [17], CASSANDRA using the LDA and CASSANDRA using the OPM exchange at 600 eV and 5.2 g/cc. The position of the experimental Ly$_\alpha$ line at ~2625 eV is fairly well matched by the OPM at ~2627 eV, but the LDA locates this feature at ~2573 eV. The position of the experimental He$_\alpha$ line is ~2461 eV and the OPM and LDA position the feature 2 eV lower and 9 eV higher in energy respectively. The gross inaccuracy in the positioning of LDA Ly$_\alpha$ line is due to the fact that the self interaction energy of the Coulomb term of Eq. (1) is not fully counteracted by the self interaction of the LDA exchange term.

To demonstrate the problems associated with self-interaction more clearly, Table 1 contains energies for a 1s-2p transition of a CASSANDRA simulation using the ground configuration of S^{+15} as the initial state. Given that there is only one bound electron, the Coulomb and exchange energies must consist entirely of self interaction energy and therefore the change in energy due to a transition from 1s-2p should result in a cancelling between the change in the Coulomb (ΔCoulomb) and change in exchange (ΔExchange) energy components, i.e. ΔCoulomb + ΔExchange =0. However, this is not the case for the LDA; the change in the OPM exchange energy (absolute magnitude) closely matches the change in the OPM Coulomb energy, the difference being ~5 eV, whilst for the LDA there is ~37 eV energy difference in these two components. This is entirely due to the LDA not accounting correctly for self interaction in the exchange calculation. To show how self-interaction energy can have a variable effect on transition energies, Table 2 contains energies for a 1s-2p transition for He-like sulfur, S^{+14}, again using the ground configuration as the initial state. For

Table 1
Atomic energies (eV) for S^{+15} for CASSANDRA LDA and CASSANDRA OPM for which the Δ energies represent a transition from 1s to 2p.

Configuration	LDA		OPM	
	S^{+15} 1s	S^{+15} 2p	S^{+15} 1s	S^{+15} 2p
Kinetic	18,139.12	15,529.54	18,307.83	15,668.32
Nuclear	−11,009.73	−5,779.70	−11,072.32	−5,809.63
Coulomb	1,858.54	1,757.86	1,863.98	1,763.30
Exchange	−312.93	−249.26	−136.06	−40.82
ΔKinetic		2,609.57		2,639.51
ΔNuclear		−5,230.03		−5,262.68
ΔCoulomb		100.68		100.68
ΔExchange		−63.67		−95.24
Transition energy		−2,583.45		−2,617.74

Table 2
Atomic energies (eV) for S^{+14} for CASSANDRA LDA and CASSANDRA OPM for which the Δ energies represent a transition from 1s to 2p.

Configuration	LDA		OPM	
	S^{+14} $1s^2$	S^{+14} 1s2p	S^{+14} $1s^2$	S^{+14} 1s2p
Kinetic	20,340.52	17,861.56	20,498.34	18,030.27
Nuclear	–17,472.44	–12,373.02	–17,535.02	–12,443.77
Coulomb	2,283.04	2,021.81	2,291.20	2,027.25
Exchange	–429.94	–331.98	–266.67	–176.87
ΔKinetic		2,478.96		2,468.07
ΔNuclear		–5,099.42		–5,091.25
ΔCoulomb		261.23		263.95
ΔExchange		–97.96		–89.80
Transition Energy		–2,457.19		–2,449.03

this case the self interaction energy of the Coulomb term is more accurately offset by the LDA exchange with the consequence that the CASSANDRA LDA and OPM transition energies are in closer agreement. A point to note here is that the transition energies of Table 1 differ by ~10 eV from those shown in Fig. 1. This is because the energies of Table 1 are single configuration-to-configuration transitions, whereas those in Fig. 1 arise from a thermal distribution of many configuration-to-configuration transitions, resulting in a 10 eV shift relative to the single configuration cases.

These simulations demonstrate the superior accuracy of the OPM when compared with the LDA exchange model and show that spurious self interaction energy is negated more effectively by the OPM exchange formulation. In general, there is price to pay for this improvement in terms of computational resources; however, this is not large in this fairly simple case. Running as a serial test case, the CASSANDRA LDA simulation finished in ~94% of the time it took to complete the CASSANDRA OPM simulation.

5.2. Niobium opacity simulation: $T \approx 40$ eV, $\rho \approx 0.025$ g/cc

At this temperature and density, niobium has an average ionization of $Z^* \approx 11$ and the plasma contains ions with a partially full M-shell and excited electrons in higher lying states. Due to the complexity of the possible configurations of open M-shell niobium, this case is a good test of inner orbital transitions, ones that originate from the K-shell or L-shell. It is within these transitions that the discrepancy in self interaction is most noticeable.

DAVROS is a detailed term accounting opacity code that uses detailed atomic physics and has been developed at AWE independent of CASSANDRA. DAVROS computes configuration energies via Slater integrals so is free from the self-interaction problem. It has been shown to be a good match for experimental data [12] and is used here as a measure of the efficacy of CASSANDRA for this test case. Fig. 2 shows a DAVROS opacity spectrum and a CASSANDRA LDA simulation with the main transition features labelled. It can be clearly seen that the LDA spectrum is systematically lower in energy than DAVROS, with the transition involving an s-state, in this instance the 2s orbital, having the largest discrepancy. Fig. 3 shows the same simulated opacity spectra from DAVROS and CASSANDRA using the OPM exchange. It can be seen that CASSANDRA OPM locates the main features in line with the DAVROS simulation, a major improvement over the LDA version. There are some differences in line strength, but it is the location of the features that is of interest here.

The price for this improved accuracy is in the time it takes to complete the simulation. Again, running as a serial test case, the CASSANDRA LDA simulation finished in ~50% of the time it took to complete the CASSANDRA OPM simulation.

5.3. Niobium simulations: GRASP2K line positions

As a further verification of CASSANDRA OPM, transition energies between fixed configurations of niobium are compared with the GRASP2K atomic physics code. The given base or initial configurations have a high probability of occurring in the niobium 40 eV, 0.025 g/cc simulation and have been selected so that transition energies from the tables may, at least approximately, be compared to Figs. 2 and 3.

Table 3 shows a base configuration and three excited configurations representing transitions of 2s1/2→4p3/2, 2p1/2→4d3/2 and

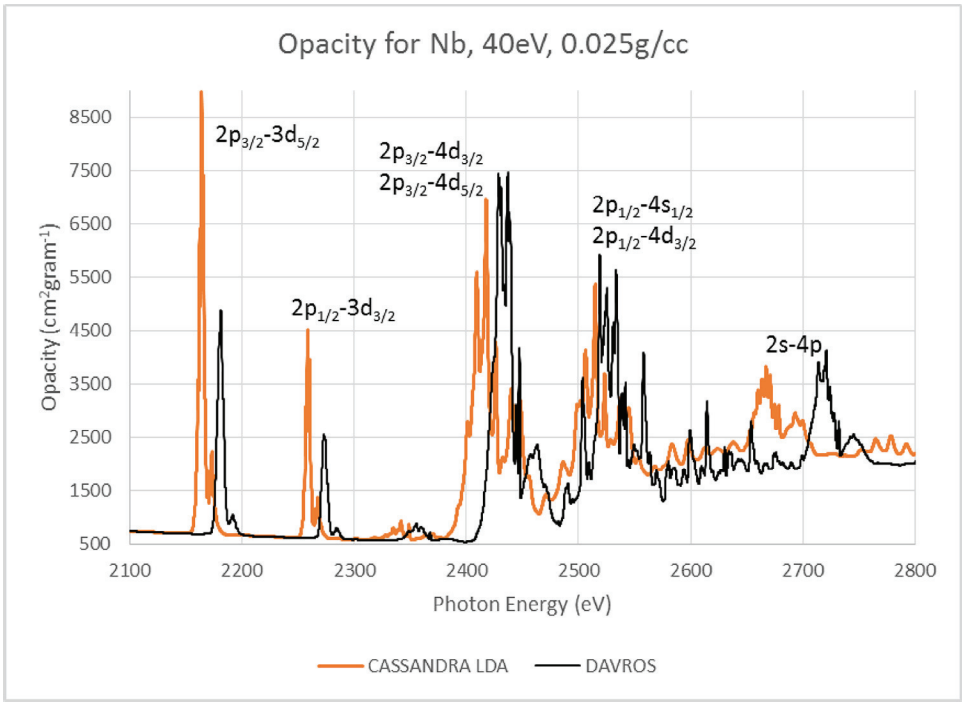

Fig. 2. Niobium opacity spectrum for transition originating from n = 2. CASSANDRA LDA and DAVROS with prominent transitions labelled.

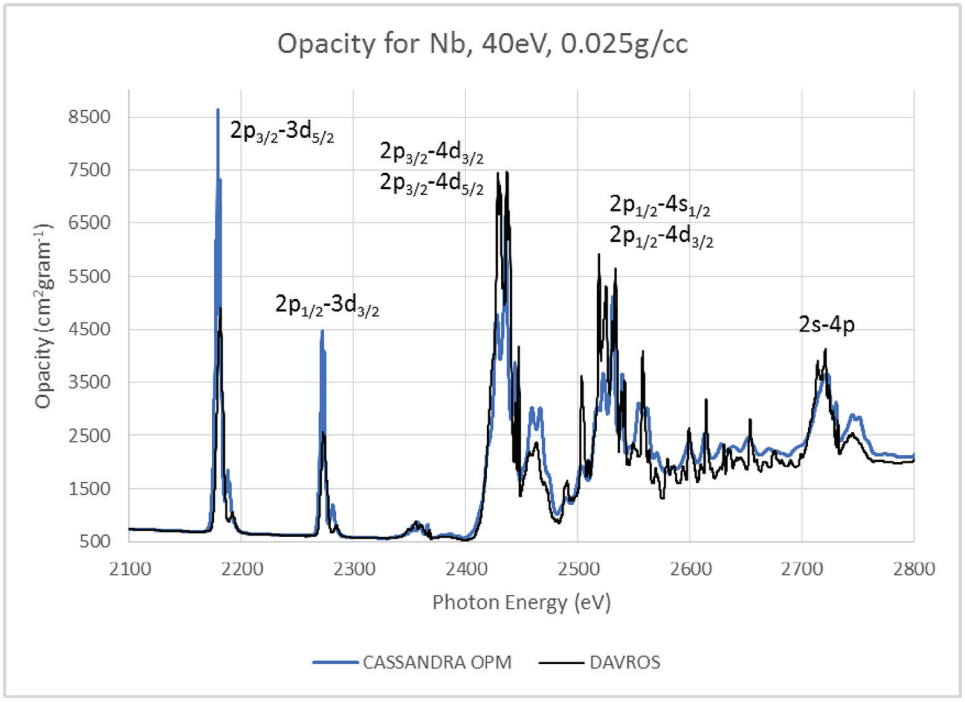

Fig. 3. Niobium opacity spectrum for transition originating from n = 2. CASSANDRA OPM and DAVROS with prominent transitions labelled.

2p3/2→4d5/2. Tables 4–6 show total and transition energies from simulations of the given configurations for GRASP2K, CASSANDRA OPM and CASSANDRA LDA. It can be seen that the GRASP2K and CASSANDRA OPM transition energies match within a few eV, whereas the discrepancies in the CASSANDRA LDA transition energies are 56 eV for the 2s→4p transition and >20 eV for the 2p→4d transitions. These discrepancies are in line with those of the niobium 40 eV, 0.025 g/cc simulation when compared to DAVROS. Table 7 shows a base configuration and two excited configurations representing transitions of 2p1/2→3d3/2 and 2p3/2→3d5/2 and Tables 8 and 9 show the associated energies. It can be clearly seen that the GRASP2K and CASSANDRA OPM transition energies are well matched, whereas the discrepancies in the CASSANDRA LDA transition energies are >15 eV. Again, these discrepancies are in line with those of the niobium 40 eV, 0.025 g/cc simulation.

Table 3
Configurations for the transition energies of Tables 4–6.

	Occupancy			
	Base configuration	2s1/2→ 4p3/2	2p1/2→ 4d3/2	2p3/2→ 4d5/2
1s1/2	2	2	2	2
2s1/2	2	1	2	2
2p1/2	2	2	1	2
2p3/2	4	4	4	3
3s1/2	2	2	2	2
3p1/2	2	2	2	2
3p3/2	4	4	4	4
3d3/2	4	4	4	4
3d5/2	6	6	6	6
4s1/2	1	1	1	1
4p1/2	1	1	1	1
4p3/2	0	1	0	0
4d3/2	0	0	1	0
4d5/2	0	0	0	1

Table 4
Energies (eV) of a 2s1/2→4p3/2 transition.

Configuration	GRASP2K	CASSANDRA OPM	CASSANDRA LDA
Base (Table 3)	–102,856.8	–102,263.1	–102,128.5
2s1/2→4p3/2	–100,140.0	–99,548.3	–99,467.7
Transition energy	–2,716.8	–2,714.8	–2,660.8

5.4. *Germanium: T = 60 eV, ρ = 0.05 g/cc*

Fig. 4 shows CASSANDRA LDA and CASSANDRA OPM simulations together with experimental data for germanium [17] with an open M-shell. At this temperature and density, germanium has an average ionization of $Z^* \approx 11$. CASSANDRA OPM locates the L-shell transitions, 2p-3d, 2s-3p and 2p-4d, in good agreement with the experiment, although the strength of the lines of the 2p-4d feature is underestimated. In contrast, CASSANDRA LDA, as in the niobium case, locates these features consistently lower in energy. The 2s-3p feature is particularly poorly located, yet again highlighting the importance of the self interaction energy when dealing with transitions involving s-states.

For this case the CASSANDRA LDA simulation finished in ~40% of the time it took to complete the CASSANDRA OPM simulation.

Table 5
Energies (eV) of a 2p1/2→4d3/2 transition.

Configuration	GRASP2K	CASSANDRA OPM	CASSANDRA LDA
Base (Table 3)	–102,856.8	–102,263.1	–102,128.5
2p1/2→4d3/2	–100,331.9	–99,740.9	–99,623.8
Transition energy	–2,524.9	–2,522.2	–2,504.7

Table 6
Energies (eV) of a 2p3/2→4d5/2 transition.

Configuration	GRASP2K	CASSANDRA OPM	CASSANDRA LDA
Base (Table 3)	–102,856.8	–102,263.1	–102,128.5
2p3/2→4d5/2	–100,423.6	–99,835.0	–99,720.6
Transition energy	–2,433.2	–2,428.1	–2,407.9

Table 7
Configurations for the transition energies of Tables 8 and 9.

	Occupancy		
	Base configuration	2p1/2→ 3d3/2	2p3/2→ 3d5/2
1s1/2	2	2	2
2s1/2	2	2	2
2p1/2	2	1	2
2p3/2	4	4	3
3s1/2	2	2	2
3p1/2	2	2	2
3p3/2	4	4	4
3d3/2	3	4	3
3d5/2	5	5	6
4s1/2	1	1	1
4p1/2	1	1	1
4p3/2	1	1	1
4d3/2	0	0	0
4d5/2	1	1	1

Table 8
Energies (eV) of a 2p1/2→3d3/2 transition.

Configuration	GRASP2K	CASSANDRA OPM	CASSANDRA LDA
Base (Table 7)	–102,381.6	–101,790.5629	–101,661.0666
2p1/2→3d3/2	–100,102.4	–99,511.2	–99,397.64409
Transition energy	–2,279.3	–2,279.3	–2,263.4

Table 9
Energies (eV) of a 2p3/2→3d5/2 transition.

Configuration	GRASP2K	CASSANDRA OPM	CASSANDRA LDA
Base (Table 7)	–102,381.6	–101,790.5629	–101,661.0666
2p3/2→3d5/2	–100,195.0	–99,604.3	–99,491.58873
Transition energy	–2,186.6	–2,186.3	–2,169.5

6. Conclusions

With the implementation of the OPM exchange model, CASSANDRA now provides a more consistent treatment of self interaction in the Coulomb and electron exchange calculations. It should be noted from the S^{+15} simulations of Table 1 that the self interaction does not cancel exactly, there being an ~5 eV difference between ΔCoulomb and ΔExchange. However, calculated transition energies are more in line with experimental data and are consistent with detailed calculations of the DAVROS opacity code and the GRASP2K atomic physics code. Also, it should be noted that the OPM exchange model, as implemented, determines the exchange potential using bound electron densities only and exhibits a 1/r Coulomb tail of an isolated ion. Further work is required to extend the exchange energy calculations to include continuum electrons and direct plasma effects, perhaps following the lead of Wilson and Liberman [18]. This may account for some of the difference in ΔCoulomb and ΔExchange for the CASSANDRA OPM hydrogenic sulfur simulations.

Processing time is a major factor for atomic physics codes, and although this was borne in mind during this implementation, there are certain overheads in the OPM exchange calculation that result in the OPM simulations taking, in general, up to 5 times longer to compute than the LDA (including simulations not reported here). However, there may be scope to further optimize the code to reduce this differential. In addition, CASSANDRA OPM has been used to calculate further opacity data as a test of reliability and has proven robust in so doing.

Acknowledgements

The CASSANDRA opacity code was developed at AWE by BJB Crowley, DKK Landeg, D Rowley, JW Harris, SJ Rose, CC Smith, LM Upcraft and M Jeffery with invaluable assistance from DA Liberman, SJ Davidson and PV Gibbons. We would like to thank BG Wilson for

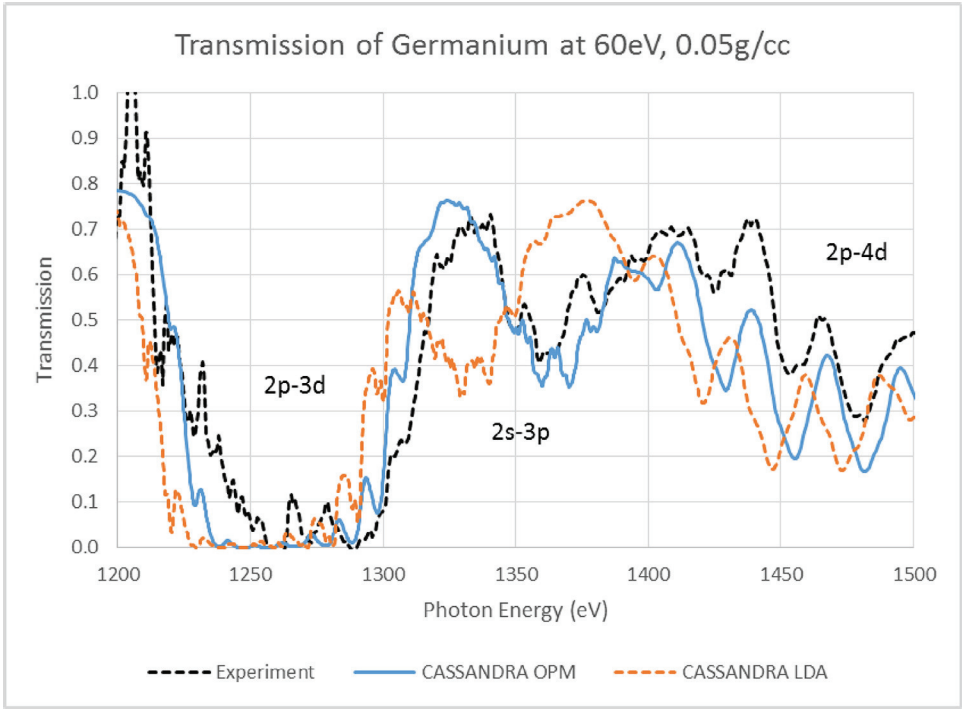

Fig. 4. Germanium transmission spectrum. CASSANDRA with the OPM and LDA exchange models compared to experiment. The LDA formalism systematically positions the absorption features lower in energy. By contrast the OPM positions the features more in line with the experiment.

valuable conversations on the OPM formalism and LM Upcraft for the DAVROS calculations.

References

[1] B.J.B. Crowley, Average-atom quantum-statistical cell model for hot plasma in local thermodynamic equilibrium over a wide range of densities, Phys. Rev. A 41 (1990) 2179–2191.
[2] B.J.B. Crowley, J.W.O. Harris, Modelling of plasmas in an average-atom local density approximation: the CASSANDRA code, J. Quant. Spectrosc. Radiat. Transfer 71 (2001) 257–272.
[3] O. Gunnarson, B.I. Lundqvist, Exchange and correlation in atoms, molecules and solids by the spin-density-functional formulism, Phys. Rev. B 13 (1976) 4274–4298.
[4] B.G. Wilson, D.A. Liberman, P.T. Springer, A deficiency of local density functionals for the calculation of self-consistent field atomic data in plasmas, J. Quant. Spectrosc. Radiat. Transfer 54 (1995) 857–878.
[5] J.P. Perdew, A. Zunger, Self-interaction correction to density-functional approximations for many-electron systems, Phy. Rev. B 23 (1981) 5048–5078.
[6] J.B. Krieger, Y. Li, G.J. Iafrate, Construction and application of an accurate local spin polarized Kohn-Sham potential with integer discontinuity: exchange only theory, Phys. Rev. A 45 (1992) 101–126.
[7] A.D. Becke, E.R. Johnson, A simple effective potential for exchange, J. Chem. Phys. 124 (2006) 221101, 1–4.
[8] J.D. Talman, W.F. Shadwick, Optimized effective atomic central potential, Phys. Rev. A 14 (1976) 36–40.
[9] J.D. Talman, A program to compute variationally optimized effective atomic potentials, Comp. Phys. Comm. 54 (1989) 85–94.
[10] B.A. Shadwick, J.D. Talman, M.R. Norman, A program to compute variationally optimized relativistic atomic potentials, Comp. Phys. Comm. 54 (1989) 95–102.
[11] M.J. Norman, J.E. Andrew, T.H. Bett, R.K. Clifford, J.E. England, N.W. Hopps, et al., Multipass reconfiguration of the HELEN Nd: glass laser at the Atomic Weapons Establishment, Appl. Opt. 41 (2002) 3497–3505.
[12] L.M. Upcraft, M. Jeffery, J.W.O. Harris, The DAVROS opacity code: detailed term accounting calculations for LTE plasmas, High Energ. Dens. Phys. 14 (2015) 59–66.
[13] P. Jönsson, X. He, C.F. Fisher, I.P. Grant, The grasp2K relativistic atomic structure package, Comp. Phys. Comm. 177 (2007) 597–622.
[14] C.C. Smith, Configuration broadening of high-Z transition array profiles, J. Quant. Spectrosc. Radiat. Transfer 59 (1998) 109–116.
[15] J.F. Janak, Proof that $\partial E/\partial n_i = \varepsilon_i$ in density functional theory, Phy. Rev. B 18 (1978) 7165–7168.
[16] R.D. Cowan, The Theory of Atomic Structure and Spectra, University of California Press, 1981.
[17] D.J. Hoarty, private communication. AWE PLC, Aldermaston, Berkshire, UK.
[18] B.G. Wilson, D.A. Liberman, Insights on the plasma polarization shift: a comparison of local density approximation and optimum potential methods, J. Quant. Spectrosc. Radiat. Transfer 54 (1995) 427–435.